Engineering Science and Technology, an International Journal 35 (2022) 101129

HOSTED BY

Contents lists available at ScienceDirect

Engineering Science and Technology, an International Journal

journal homepage: www.elsevier.com/locate/jestch

# Surface roughness impact on the performance of the 3D metal printed waveguide coupler at millimeterwave band

Muataz Almeshehe [a,*], Noor Murad [a], Mohamad Rahim [a], Osman Ayop [a], Noor Samsuri [a], Mohamad Abd. Aziz [b], Mohamed Osman [c]

[a] Advanced RF & Microwave Research Group (ARFMRG), School of Electrical, Engineering, Faculty of Engineering, Universiti Teknologi Malaysia (UTM), 81310, UTMJB, Johor, Malaysia
[b] Faculty of Electronic and Computer Engineering, Universiti Teknikal Malaysia Melaka (UTeM), Hang Tuah Jaya, 76100, Durian Tunggal, Melaka, Malaysia
[c] School of Computer and Communication Engineering, Universiti Malaysia Perlis (UniMAP), Pauh Putra Campus, 02600 Arau, Perlis, Malaysia

ARTICLE INFO

*Article history:*
Received 8 May 2021
Revised 6 December 2021
Accepted 15 February 2022
Available online 25 February 2022

*Keywords:*
3D metal printing
Millimeterwave
Surface roughness
Waveguide coupler

ABSTRACT

This paper presents the impact of surface roughness on the performance of a three –dimensional (3D) metal printed waveguide coupler designed at 28 GHz. The surface roughness is a significant factor that may affect 3D printed structures and post processing may be needed. It may degrade the performance of the printed devices in term of the reflection coefficient and increases the insertion loss. Thus, this work analyses the surface roughness impact on the 3D metal printed coupler designed at 28 GHz. The hybrid coupler is a waveguide-based structure with coupled resonators and the coupling is controlled by tuning the iris dimensions. The measurement is done without any post processing procedure to ensure the validation of the printed coupler with simulation results. The surface roughness measurement is performed with six tested areas of coupler structure using advanced 3D optical microscope. Then, the measured surface roughness values are included in CST software to re-simulate and compare with the original and measured results. The analysis shows that the surface roughness has a moderate influence on the reflection coefficient with 7 dB loss and 0.7 dB increased in insertion loss at 28 GHz.


## 1. Introduction

Millimeterwave technology has emerged in recent years as a promising technology for future to support the capacity and speed of information transfer. At millimeterwave frequencies, fabrication or manufacturing of devices is seen as a significant challenge as the devices overall dimension are shrink with the shorter wavelength. It is crucial to have a good tolerance of manufacturing with high-precision machining, and low cost of fabrication [1]. Currently, the manufacturing techniques used in microwave and millimeterwave devices are categorized into traditional subtractive manufacturing (SM) and additive manufacturing (AM). Commonly, SM techniques are divided and not limited to four main types such as computer numerical control (CNC), laser machining, micromachining, and electrical discharge machining (EDM) [2]. The EDM technique uses the electrical discharge to etch the metal plate into the intended form. However, the processing cycle is taken long time to produce the desired form [3]. CNC machining cut out of bulk metal to the desired form by using computer precision. Additionally, CNC requires an expert and skilled technician to ensure a high precision fabrication process and devices. Moreover, the fabrication tolerance is less acceptable than EDM technique in terms of producing surface roughness, dimensional tolerance, or both [3]. Thus, SM techniques have a significant challenge when it employs in the fabrication of millimeterwave devices. These challenges can be concluded as low material profile, long processing cycle, high dimensional and surface roughness profiling, and high cost of fabrication. Hence, an urgent alternative to resolve these challenges is needed in both research and industrial fields.

Additive manufacturing or 3D printing is proposed as an alternative solution to overcome SM techniques challenges in manufacturing millimeterwave devices [4]. AM has the benefits over traditional SM techniques in terms of low power consuming, shorter processing cycle, high material utilization, the capability of printing very complex structures, less material waste, friendly environment and low cost. In millimeterwave technology, the usage of AM techniques can be seen in passive devices such as waveguide-based structures, planar antennas and devices, filters, and cavity-resonators structures [5,6]. Generally, AM techniques print the structure layer by layer at each time using liquid or powder-based materials [5]. The techniques are classified into

* Corresponding author.
Peer review under responsibility of Karabuk University.

https://doi.org/10.1016/j.jestch.2022.101129
2215-0986/

dielectric material such as Fused Deposition Modelling (FDM), and metal material such as Direct Metal Laser Sintering/Melting (DMLS/M), Electronic Beam Melting (EBM), and Selective Laser Melting (SLM) [6]. Each technique has the features and drawbacks based on their cost, build speed, geometry limitations, resolution, and surface finishing [7].

Several studies are presented on the effects of 3D printing techniques and surface roughness on the performance of passive devices [8–13]. These studies highlighted the most critical issues in 3D printing which are the surface roughness and low dimensional tolerance [8]. As surface roughness is significantly important in millimeterwave antennas and devices where substantial losses are expected. It degrades the performance of the printed devices at high frequencies in term of reflection coefficient and isolation. In addition, it increases the insertion loss [9]. In instance, a study on the effects of surface roughness on radiation characteristics and matching impedance for rod antenna is proposed in [10]. It highlighted that the surface roughness affected the optimal design by shifting the E-filed intensity along the antenna rod and limited the printing resolution. Another study is introduced for a compact 3D printed magnetic reflectors for millimeterwave application in [11]. It highlighted the effects of the low surface roughness at 100 GHz in degrading the performance of reflectors. A metallic 3D printed large antenna array for satellite application at 20 GHz is presented in [12]. The authors focused on the advantages of using metallic 3D printing in high frequency. However, the surface roughness found in the fabricated prototype degrades the radiation pattern and gain performance. Recently, a low cost 3D printed directional coupler at 2 GHz is investigated in [13]. The results show that when the level of the surface roughness is small, the power losses an insertion loss are lower than the acceptable level. Thus, SM techniques have a significant challenge when it employs in the fabrication of millimeterwave devices. These challenges can be concluded as low material profile, long processing cycle, high dimensional and surface roughness profiling, and high cost of fabrication. Hence, an urgent alternative to resolve these challenges is needed in both research and industrial fields.

Hence, this paper presents a study on the impact of the surface roughness on a 3D printed waveguide coupler at 28 GHz. The prototype is metal printed using SLM printer. The investigation involves the effects of the surface roughness on the performance of the 3D printed air-filled waveguide-based coupler with rectangular cavity resonators. In addition, this paper is a research extension on the waveguide coupler that has been proposed in our work in [14]. The paper structure is divided as follow; section two discusses the coupler design and fabrication with performance validity. Then, a briefly introduction on the surface roughness measurement method. Section 3 presents the results obtained from the surface roughness measurement process with the impact of obtained results on the coupler characteristics. Conclusion of the work can be found in Section 4.

## 2. Design, Fabrication, and surface roughness method

This section discusses the design of 3-dB hybrid coupler based on rectangular air-filled waveguide-based structures with rectangular iris coupling method. A hybrid coupler is a device that has two inputs and two outputs. It provides an equal divided power of – 3 dB with 90° or 180° phase difference at output ports. It is widely used in microwave and millimeterwave applications specifically in antenna beamforming network such as Butler matrix, Blass matrix, and Nolen matrix [14,15]. It controls the phase shifting and the coupling factor at these beamforming matrixes output. Hence, an accurate design and fabrication of a hybrid coupler especially at millimeterwave bands is required. The general form of a hybrid coupler is presented in Fig. 1. The characteristics of the coupler are defined from its S-parameters; reflection coefficient from input port 1 ($S_{11}$), transmission coefficients at outputs ($S_{21}$ and $S_{31}$), and isolation coefficient from port 4 ($S_{41}$). Another significant characteristic is the phase progressive difference at outputs ($\angle S_{31}$-$\angle S_{21}$). The proposed 3-dB coupler is designed by using air filled rectangular waveguide cavity resonator structure with high quality factor and extraction of its coupling coefficients as in [14].

A cavity resonator is defined as a section from a rectangular waveguide-based structure, where both ends are shorted circuit as illustrated in Fig. 2 [15]. The transverse mode (TE) of a rectangular cavity resonator is defined as the dominant mode ($TE_{101}$). Due to the lowest resonance of the frequency mode. In this study, the rectangular cavity resonator is assumed to be air filled. The standard waveguide-based structure inner dimension is chosen to be WR-28 as a reference in designing the waveguide cavity resonator and the iris coupling structure. Where the inner dimension of WR-28 ($a \times b$) is 7.112 mm × 3.556 mm. The length of the cavity resonator ($d$) is calculated by [14].

$$\beta_{10} d = l\pi \text{ when } l = 1, 2, 3, \quad (1)$$

where, ($\beta_{10}$) is the $TE_{10}$ propagation constant mode, and $l$ is the number of the cavity resonator used. To find the propagation constant mode ($\beta_{10}$), the guided wavelength ($\lambda_g$) of the waveguide cavity resonator is firstly obtained by [14].

$$\beta_{10} = \sqrt{k^2 - \left(\frac{m\pi}{a}\right)^2 - \left(\frac{n\pi}{b}\right)^2} \quad (2)$$

$$\lambda_g = \frac{2\pi}{\beta_{10}} \quad (3)$$

where, $k = \omega\sqrt{\mu_0 \varepsilon_0}$. Since this work in on air-filled rectangular cavity resonator, the dissipated energy is only considerate from electrical walls (conductor loss) of the waveguide structure. The external quality factor is controlling the resonant frequency and the fractional bandwidth between the ports of the coupler and the cavity resonators. In other words, it controls the reflection, isolation, and transmitting coefficients of the coupler. The coupling coefficients

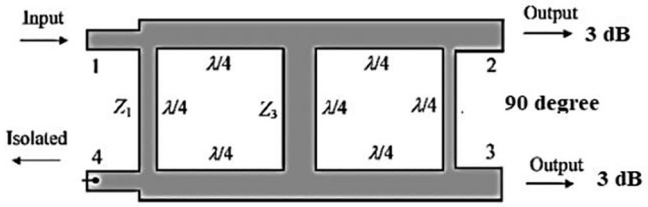


**Fig. 1.** General form of 3-dB hybrid coupler [14].

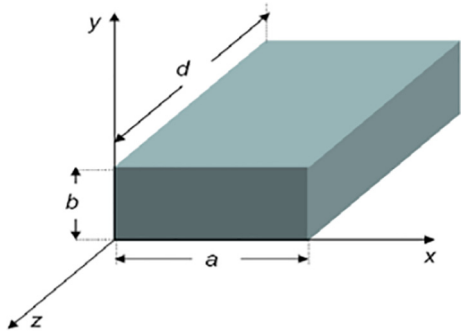


**Fig. 2.** Rectangular waveguide cavity resonator configuration [15].

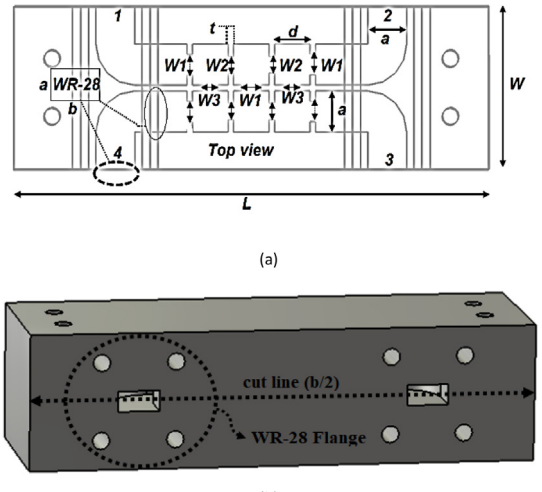


**Fig. 3.** (a) 3-dB coupler dimensions, ($a$ = 7.112, $b$ = 3.556, $d$ = 8.2, $L$ = 78.2, $W$ = 28.22, $W1$ = 3.544, $W2$ = 2.850, $W3$ = 2.750, *and* $t$ = 1) (dimensions are in mm). (b) b/2 line cut for fabrication process.

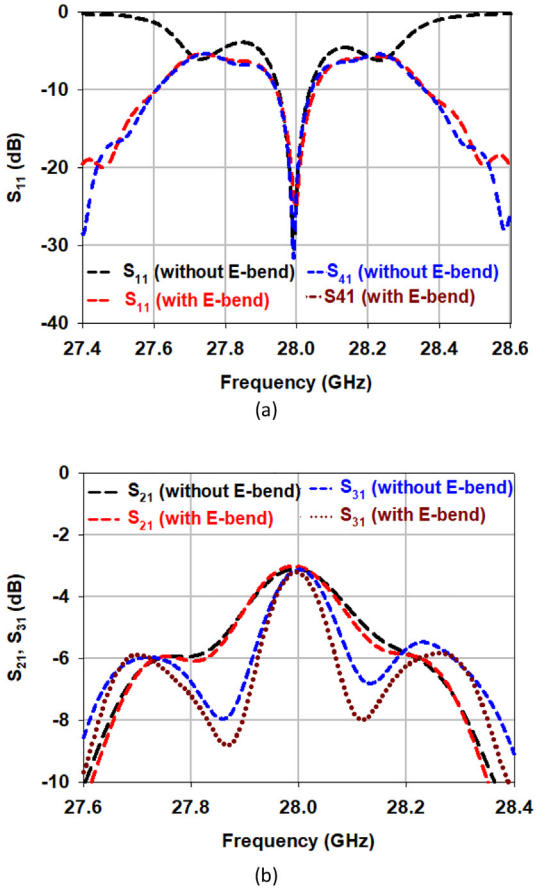


**Fig. 4.** Simulation response of the proposed coupler with and without E-bends. (a) Reflection and isolation coefficients. (b) Transmission coefficients.

of the cavity resonator is managed by using iris air-filled rectangular coupling structure. By tuning this iris, it can be achieved the required 3-dB coupling at output ports [14,15]. Fig. 3 (a) shows the proposed 3-dB coupler with six cavity resonators implementation after the calculations of its parameters. The coupler is fed with

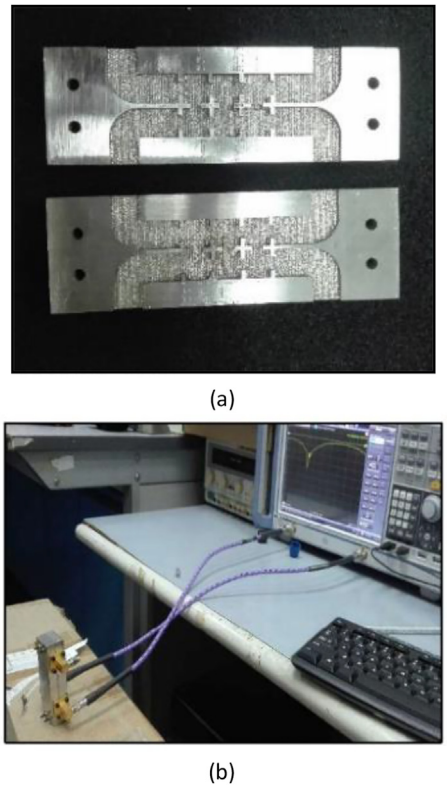


**Fig. 5.** 3-dB coupler prototype. (a) Printed into two pieces and attached together by M3 bolts, (b) measurement setup.

four 90° E-bend with 11.7 mm of radius dimension. These added E-bends are for fabrication and measurement process. The designed coupler is split into two pieces (b/2) for the fabrication process to ensure a capability of surface roughness measurement and all cavities formed well as shown in Fig. 3 (b).

In order to analyse the effects of adding four E-bends to the coupler structure, a series of simulation process are performed in terms of S-parameter and phase difference. Fig. 4 illustrates the simulation responses of the proposed 3-dB coupler, in terms of reflection coefficient, transmission coefficient, and phase difference at 28 GHz. As can be seen from Fig. 4 (a), the effects of adding E-bends at the coupler port 1 and port 2 has a slightly difference on the coefficient and isolation coefficient with respect to coupler without E-bends.

The reflection and isolation coefficient with E-bends ($S_{11}$ and $S_{41}$) have a value of −28 dB and −32 dB respectively at 28 GHz. With respect to the coupler without E-bends the reflection and isolation coefficient are −31 dB and −32 dB correspondingly at 28 GHz. The transmission coefficients of the coupler (with and without E-bends) have similar value of −3.1 dB as shown in Fig. 4 (b). The phase progressive difference of the coupler (with and without E-bends) is 90.2° and 90° respectively. This indicates that adding E-bends at 28 GHz have no much effects on the coupler characteristics.

Fig. 5 shows the printed 3-dB coupler manufactured using metal 3D printing SLM 125 HL printer. The material deployed in the fabrication of the 3-dB coupler is Cobalt-Chromium (CoCr) material. The prototype has a sturdy structure with all ports and cavities formed well. Then, the two structures are combined with M3 bolt to form a complete coupler with a very low dimensional tolerance at inner dimension of ($a \times b$). The dimensional tolerance of (7.110 mm × 3.554 mm) is reported with respect to WR-28 of (7.112 mm × 3.556 mm). The measurement is done with using the

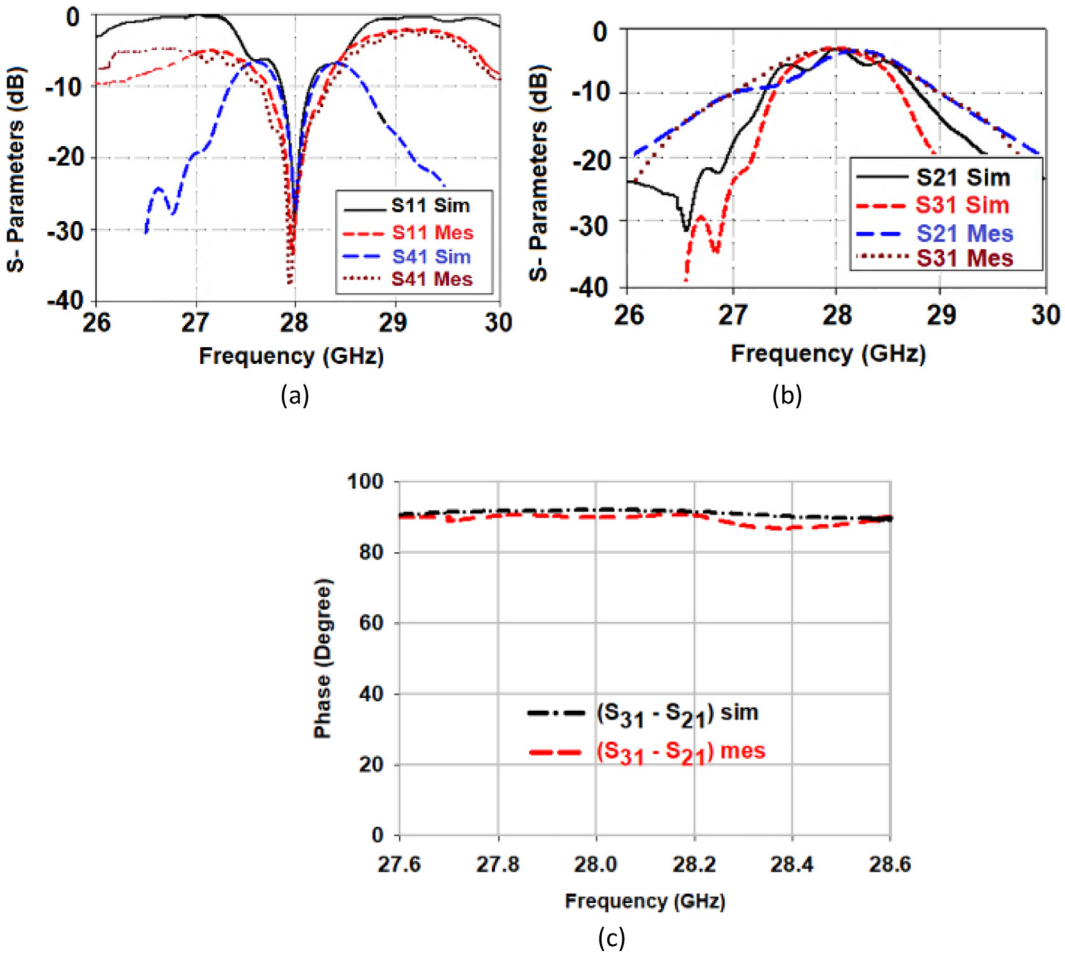


**Fig. 6.** The performance of the 3D metal printed coupler: (a) Reflection and isolation coefficients. (b) Transmission coefficients. (c) Phase Progressive difference.

**Table 1**
Cobalt chromium (CoCr) material priorities.

| Material name | Composition | Density | Melting temperature | Electrical conductivity |
|---|---|---|---|---|
| Cobalt chromium (CoCr) | 60–75 % of Cobalt, chromium of 30 %. | 10 g/cm$^3$ | 1330° | 55 % ±0.125 |

**Table 2**
Skin depth of CoCr material.

| Frequency | Calculated | Measured |
|---|---|---|
| 27 GHz | 0.512 μm | 0.498 μm |
| 28 GHz | 0.495 μm | 0.478 μm |
| 29 GHz | 0.472 μm | 0.462 μm |

R&S®ZNB40 VNA with two port cables. During calibration, a loss of 0.5 dB in cables are observed. Two terminal loads are used in every stage of measurement due to the limitation of the port number provided by the mentioned VNA.

The performance of the printed 3-dB coupler is shown in Fig. 6. The measured reflection coefficient ($S_{11}$) of −25 dB at 28 GHz is obtained as shown in Fig. 6 (a). With respect to the simulated reflection coefficient ($S_{11}$) of −28 dB, a loss of – 3 dB is observed. As mentioned previously the cable loss during calibration is about −0.5 dB, with the obtained dimensional tolerance and the surface roughness (which not yet investigated), the loss of −3 dB in reflection coefficient can be elaborated based on these factors. The measured isolation of less than −20 dB is obtained at the same

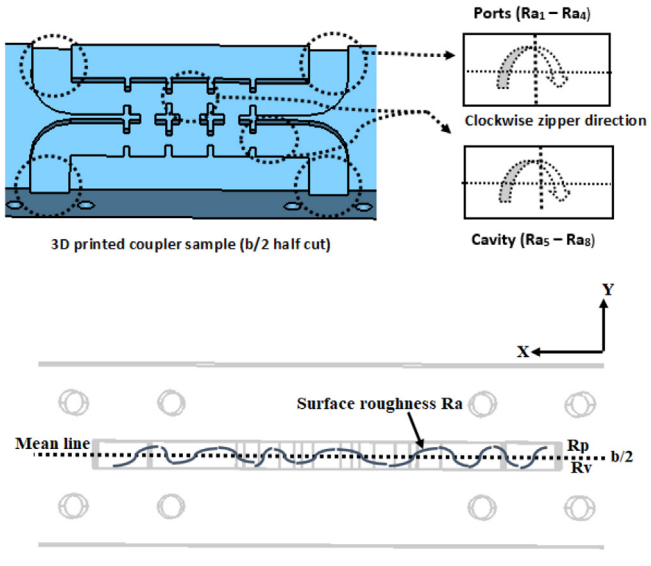


**Fig. 7.** Procedure of surface roughness measurement.

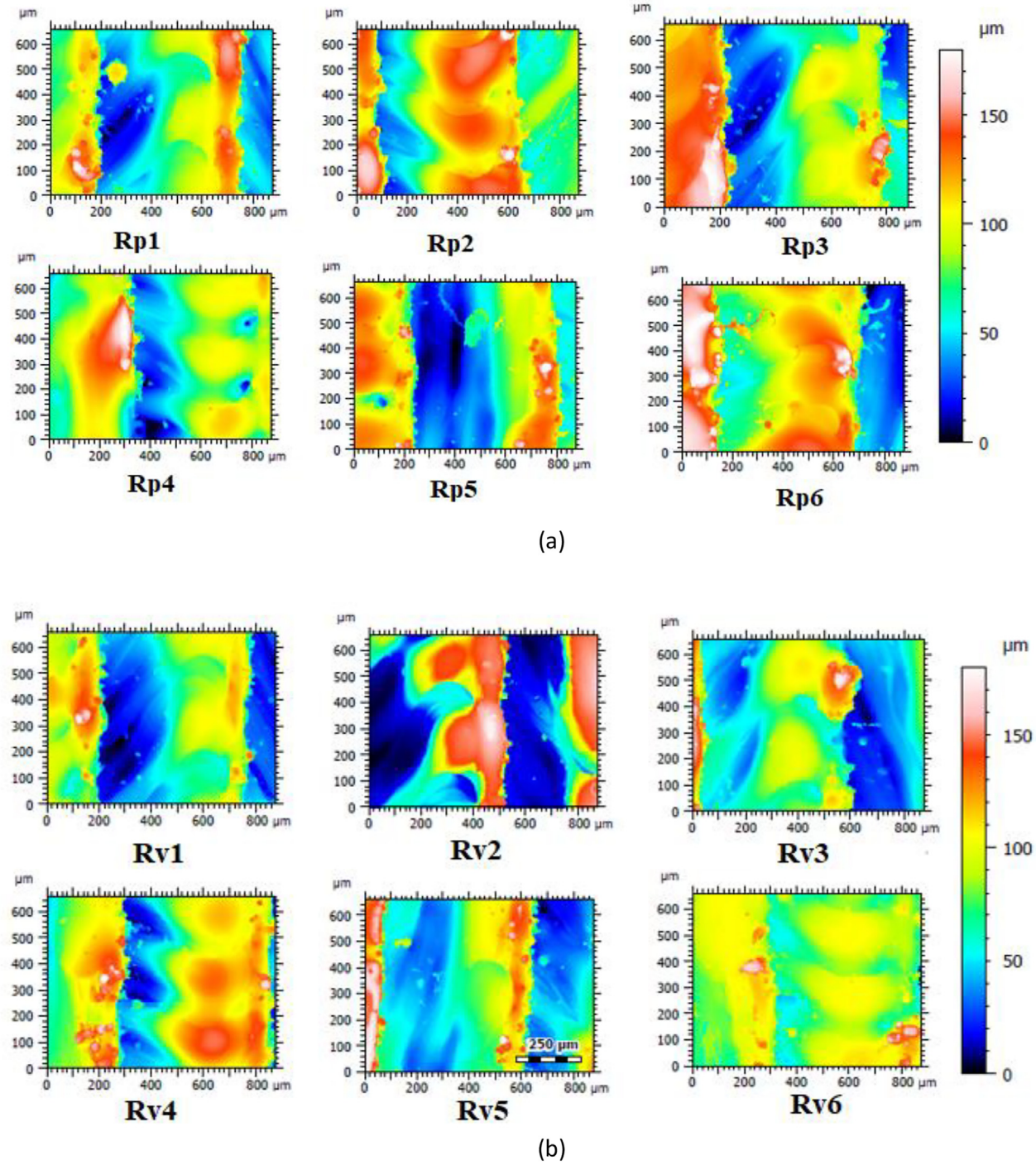


**Fig. 8.** 2D Surface roughness results for 3D printed coupler. (a) Sample 1, (b) Sample 2.

**Table 3**
Surface roughness results of the two samples of 3D printed coupler (All dimensions in µm).

| Test point | Sample 1 | Test point | Sample 2 | Full area | Value |
|---|---|---|---|---|---|
| $Rp_1$ | 30.57 | $Rv_1$ | 23.77 | $Ra_1$ | 27.17 |
| $Rp_2$ | 33.28 | $Rv_2$ | 33.36 | $Ra_2$ | 33.32 |
| $Rp_3$ | 33.32 | $Rv_3$ | 25.89 | $Ra_3$ | 29.60 |
| $Rp_4$ | 23.31 | $Rv_4$ | 21.49 | $Ra_4$ | 22.40 |
| $Rp_5$ | 60.84 | $Rv_5$ | 19.69 | $Ra_5$ | 40.26 |
| $Rp_6$ | 86.54 | $Rv_6$ | 90.23 | $Ra_6$ | 88.38 |
| Mean Rp | 44.64 | Mean Rv | 37.73 | Mean Ra | 40.18 |

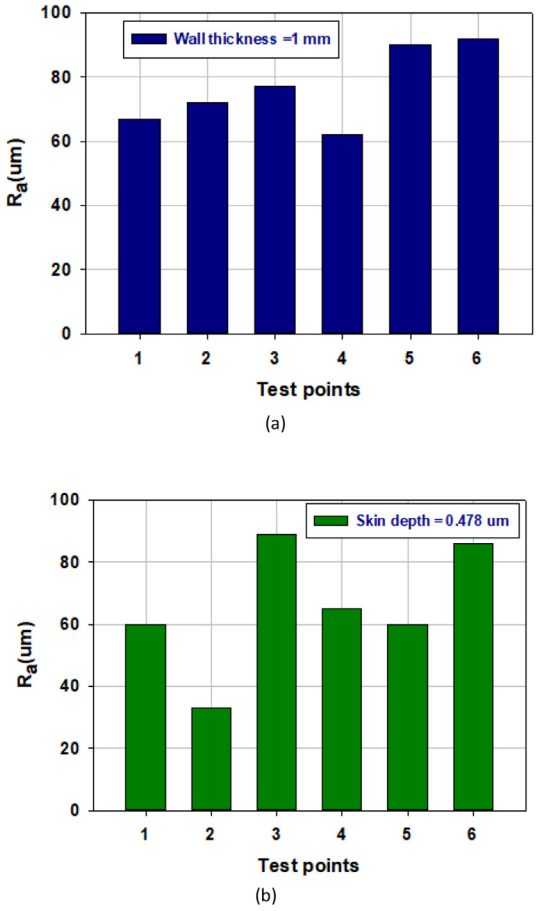


**Fig. 9.** Surface roughness profile with wall thickness and skin depth from sample 1. (a) Wall thickness = 1 mm. (b) skin depth = 0.478 μm).

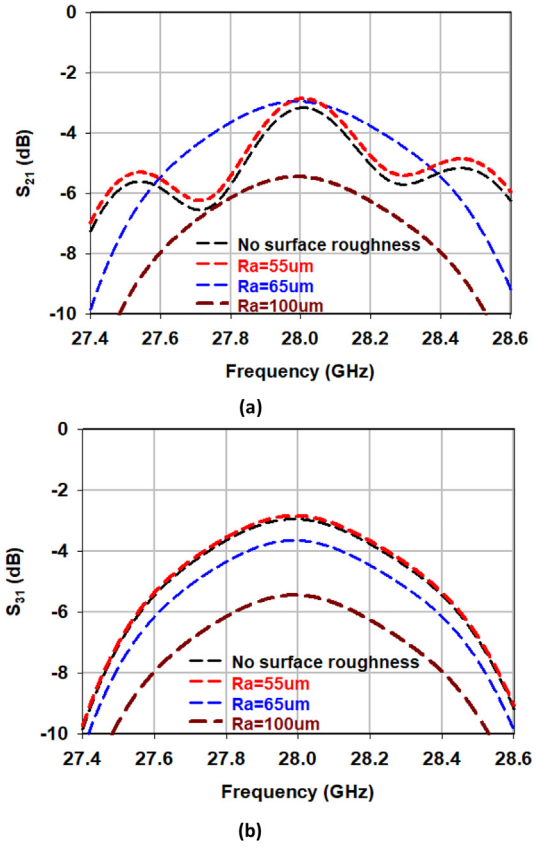


**Fig. 10.** Performance of the 3D printed waveguide coupler with different surface roughness value in terms of insertion loss ($S_{21}$) and coupling ($S_{31}$).

frequency. The measured transmission coefficient ($S_{21}$ and $S_{31}$) has been compared with the simulated ones. A power imbalance of 0.6 dB around 3.12 dB is achieved at 28 GHz with a phase difference of 87.3° as shown in Fig. 6 (b) and Fig. 6 (c) respectively.

As previously mentioned, the designed coupler is metal printed using 3D printing selective laser melting technique (SLM). This type of printer (SLM 125 HL) uses metal powder melting technique. The Cobalt chromium (CoCr) material is used in the fabrication of the designed coupler. CoCr material exhibit high casting ability with optimized high electrical conductivity, and it can provide sturdy structures with good resistance to weather conditions. The CoCr metal powder is melting at 1330° with density of 10 gm/cm$^3$. In addition, the electrical conductivity of CoCr is 55% ± 0.125. This is provide a high casting and electrical conductivity to the coupler. Table 1 summaries the CoCr material powder properties.

The skin depth of the CoCr material used in deploying 3D printed coupler is profiled and examined by field emission scanning electron microscope (FE-SEM). A skin depth layer of 10 μm is measured at all the ports and cavity layers. The obtained skin depth is used for measuring the metal thickness depth of the printed coupler. To compare the obtained metal thickness of the structure, the skin depth of the metal can be calculated by [16].

$$\delta = \sqrt{\frac{\rho}{\pi f_0 \mu_0 \mu_r}} \tag{4}$$

where, $\rho$ is represented the resistivity of the material, $f_0$ is the desired frequency, $\mu_r$ is the relative permeability, and $\mu_0 = 4\pi \times 10^{-7}$. Table 2 presented the comparison of calculated and measured skin depth of CoCr material at different frequencies for 3D printed coupler at 27 GHz, 28 GHz, and 29 GHz.

Once the skin depth of the printed material is obtained, the surface roughness is measured using 3D optical surface profile model (NewViewTM 9000). The surface roughness is evaluated in terms of arithmetic average of surface roughness profile (*Ra*). Six surface roughness measurements areas are taken for each 3D printed coupler samples. There are two samples of 3D printed coupler (as in Fig. 5 (a)). The areas are divided into four ports areas of the coupler and two areas of cavity resonators as shown in Fig. 7. The measurements of ($R_a$) at each sample are taken from top view with clockwise direction.

## 3. Results

### 3.1. Surface roughness profiling results

The surface roughness results obtained for the two samples are shown in Fig. 8. Their mean values in terms of surface roughness profile ($R_a$) are listed in Table 3. The obtained values are slightly higher compared to other conventional fabrication techniques such as machining. At all tested points for each sample, the surface roughness is higher than 12 μm [17]. Moreover, it is important to notice the range of the obtained surface roughness values from the two samples at all points. The samples 1 and 2 are tested above and below mean line with maximum peak height and valley depth surface roughness ($R_p$) and ($R_v$) respectively. The mathematical form for calculating ($R_p$), ($R_v$) and mean $R_a$ is found by [17].

$$R_{pi} = \frac{\sum_{i=1}^{n} R_{pi}}{n} \tag{5}$$

$$R_{vi} = \frac{\sum_{i=1}^{n} R_{vi}}{n} \tag{6}$$

$$R_{ai} = R_{pi} + R_{vi} = \frac{\sum_{i=1}^{n} R_{ai}}{n} \tag{7}$$

From Table 3 and Fig. 8, it can be observed that the lowest value of the surface roughness ($R_p$) of sample 1 at each test point varies between (23.31 μm) and (86.54 μm) compared to the values from sample 2 ($R_v$) ranging between (19.69 μm) and (33.36 μm). However, the mean surface roughness ($R_a$) for the whole sample (coupler) is (40.18 μm).

The surface roughness obtained results from the two samples are selected with wall thickness of 1 mm and skin depth of 0.478 μm. To evaluate the influence of the wall thickness and skin depth on the surface roughness, ANOVA test [18] is performed on the obtained surface roughness with selected value of wall thickness and skin depth as illustrated in Fig. 9. For simplicity, only results obtained from sample 1 is plotted.

It is possible to observe that the lowest surface roughness obtained from the test is between (62 μm to 77 μm) at tested point of ($Ra_1$ to $Ra_4$) for a wall thickness of 1 mm as in Fig. 9(a). This indicates that how wall thickness has a possible effect on surface roughness. Similar results are observed when applying skin depth on surface roughness as in Fig. 9 (b). It concludes that both wall thickness and skin depth of the material have significant impact on surface roughness. Hence, these two factors should be furtherly studied in detail for lower surface roughness with different values of wall thickness and skin depth. In that case, different surface roughness values are inserted in CST software and re-simulate the coupler to obtain the acceptable value of surface roughness. The values of surface roughness are ranged from minimum of 50 μm to maximum of 100 μm, taking in consideration the tested value from measurement. Fig. 10 illustrates the responses of the coupler and the effects of different surface roughness values on the coupler performance. It can be noticed from the obtained results that the acceptable value of surface roughness for optimal performance of the coupler is (55 μm) at 28 GHz. In which the coupling factor with insertion loss is around 3.05 dB at this particular value. Hence, this value of surface roughness could be considered in further future study and analysis. For this work, the previously mentioned value (62 μm to 72 μm) is used for analyzing the coupler performance in the next sub-section.

### 3.2. Impact of surface roughness on the printed coupler

Applying the surface roughness values in CST software for analysing the effects on the coupler characteristics. A series of simulations are done and the results are compared with measured responses of the printed coupler. Fig. 11 shows the characteristics of the 3-dB printed coupler in terms of reflection, transmission, and isolation coefficients. It can be seen from the comparison results that the impact of the surface roughness on the reflection coefficient is moderate with a loss of 8 dB in $S_{11}$ value with respect to no surface roughness included (as in Fig. 11 (a)). However, on isolation port no much effect happened when surface roughness is applied (as in Fig. 11 (b)). In addition, when surface roughness is applied on both port 2 and port 3, the transmission coefficients is increased by 0.7 dB. Which is with limits of impedance balance of 0.6 dB at outputs as in Fig. 11 (c) and Fig. 11 (d) respectively.

However, it can be noticed that the measured value for S21 and S31 compared to the values of surface roughness when applied to the simulation is slightly different with error of 0.8 dB. This is due to two reasons. The first reason is the assumption of no dimen-

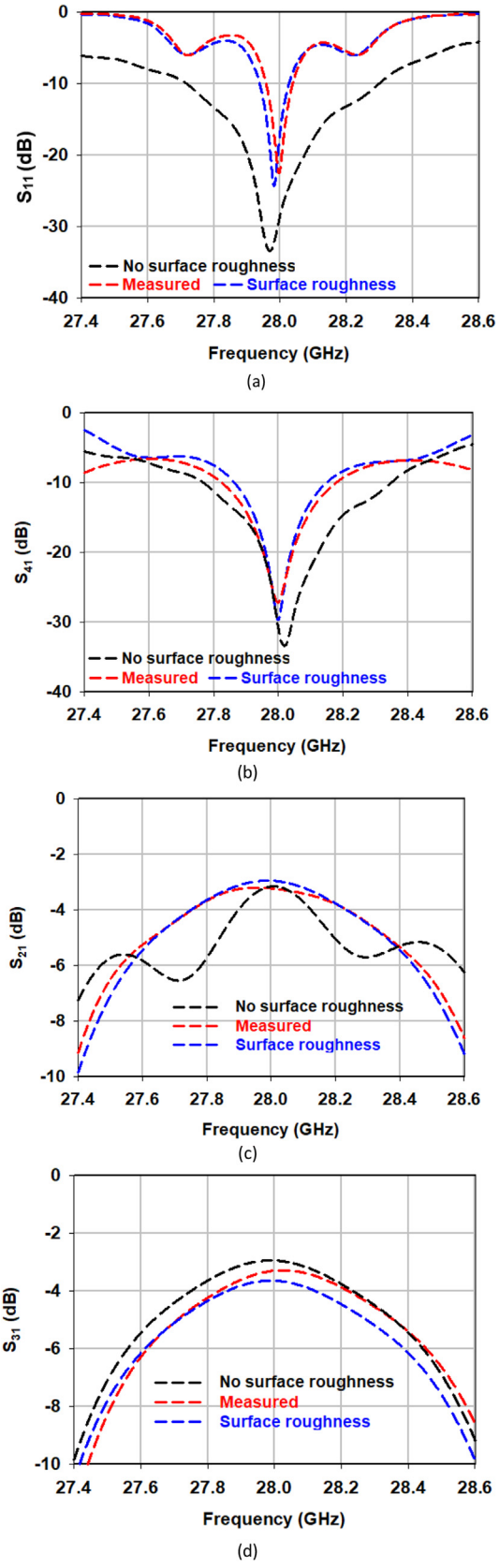


**Fig. 11.** Performance of the 3D printed waveguide coupler with surface roughness (mean Ra) included. (a) Reflection coefficient at port 1. (b) Isolation coefficient at port 4. (c) Transmission coefficient at port 2. (d) Transmission coefficient at port 3.

**Table 4**
Performance comparison with surface roughness included in the 3D printed waveguide coupler.

| Parameters | NO surface roughness | Surface roughness | Measured |
|---|---|---|---|
| Reflection coefficient ($S_{11}$) | −28 dB | −19 dB | −25 dB |
| Transmission coefficient ($S_{21}$) | −3.1 dB | −3.8 dB | −2.9 dB |
| Transmission coefficient ($S_{31}$) | −3.1 dB | −3.7 dB | −3.1 dB |
| Isolation coefficient ($S_{41}$) | −32 dB | −24.8 dB | −25 dB |
| Phase difference at outputs | 90.2° | 91.6° | 87.3° |

**Table 5**
Performance comparison with other printed coupler in respect with SM manufacturing.

| Reference | [19] | [20] | [21] | [22] | This work |
|---|---|---|---|---|---|
| Frequency | Ka-band | Ka-band | Ka-band | Ka-band | 28 GHz |
| Coupler type | Waveguide | CMOS | RGW | Microstrip/slot | Waveguide |
| Reflection | −20 dB | −15 dB | −20 dB | −18 dB | −25 dB |
| Isolation | −27 dB | −17 dB | −24 dB | −20 dB | −25 dB. |
| coupling | 1.85 dB | 2.5 dB | 4 dB | 5.2 dB | 3.1 dB |
| Phase.diff | 75° | 84° | 87° | 85° | 87.4° |
| Phase error | 15° | 6° | 3° | 4° | 2.6° |
| Fabrication | CNC | P-Well | CNC | SM | 3D printing |

**Table 6**
Performance comparison with other 3D printed coupler in respect with AM manufacturing.

| Reference | [23] | [24] | [25] | [26] | This work |
|---|---|---|---|---|---|
| Frequency | 115–150 GHz | V-band | E-band | Ku-band | 28 GHz |
| Coupler type | waveguide | Waveguide | Waveguide | Slot | Waveguide/cavity |
| Reflection | −15 dB | −14 dB | −20 dB | −20 dB | −25 dB |
| Isolation | −15 dB | −18 dB | −20 dB | −24 dB | −25 dB. |
| coupling | 3.8 dB | 4 dB | 4 dB | 6 dB | 3.1 dB |
| Phase.diff | 50° | 82° | 80° | N/A | 87.4° |
| Phase error | 40° | 8° | 10° | N/A | 2.6° |
| 3D printing | DLP | SLA | SLA | PLA | SLM |
| Post-Processing | No | Yes | Yes | Yes | No |

sional error is taken in the simulation process. The second reason is some inaccuracy in measurement due to using H-plane of the waveguide. Which results in low insertion loss at 28 GHz. The phase difference at the outputs is slightly changed to 91.6° with 4.3° phase error when surface roughness is applied. Therefore, it achieves a low loss waveguide-based coupler by using 3D SLM metal printing technique with surface roughness included. This is could be an excellent alternative for good performance millimeter-wave state of art devices. Table 4 shows the comparison of coupler performance with and without surface roughness applied.

### 3.3. Comparison with related works

The printed coupler is compared with other related works in terms of SM and AM manufacturing techniques. Table 5 summarizes the performance of several couplers that fabricated using CNC-machining and P-well technique with respect to the proposed 3D printed coupler. The comparison concludes that the proposed 3D printing technique for waveguide coupler has the advantages over other SM techniques. The coupler has better reflection, isolation, and coupling compared to existing printed SM couplers. Table 6 shows a comparison between several 3D printed coupler (using non-metal material) with the proposed 3D metal printed coupler using SLM technique. The proposed 3D printed coupler with SLM printing technique has better performance in reflection and coupling ratio at output ports. The phase difference error of 2.6° at outputs is obtained taking in consideration that no post-processing is done to the coupler using this technique. Overall, this 3D printed coupler using SLM technique has better performance with respect to other printed couplers that presented in Table 5 and Table 6 respectively.

## 4. Conclusion

This paper presented the impact of surface roughness on a 3D printed waveguide cavity resonator hybrid coupler at 28 GHz. The coupler is designed based on rectangular air-filled cavity resonator and fabricated using 3D SLM 125 HL printer with CoCr material. Then, six areas are measured for surface roughness including the input/output ports and two cavities. The measured surface roughness values are included in the coupler simulation using CST software and compared with measured and original simulated response (without surface roughness). It is found that the surface roughness comes from using SLM 125 HL printer with CoCr material has moderate impact on the coupler characteristics. A loss of 7 dB in reflection coefficient is observed from the surface roughness value from input port 1 at 28 GHz. For the outputs port 2 and port 3, a loss of 0.7 dB is reported comes from the surface roughness. Despite these losses, the 3D printed hybrid coupler has a good performance by using SLM printing technique. This could benefit the efforts for realizing a reliable performance of millimeterwave devices.

## Declaration of Competing Interest

The authors declare that they have no known competing financial interests or personal relationships that could have appeared to influence the work reported in this paper.

## Acknowledgments

This research has received funding from Universiti Teknologi Malaysia and Research Management Centre (RMC) with the support of the Collaborative Research Grant under no 04G72, 04G65, 04G67, 13J86, and 04G69. The authors acknowledge Ministry of Education (MOE), Advanced RF Microwave Research Group (ARFMG), School of Electrical Engineering, Faculty of Engineering, and UTM University-Industry Research Laboratory (T03) for given support to conduct the fabrication and experiments.

## References

[1] S. Verploegh, Passive and Active Component Design and Analysis for Millimeter Wave Front Ends (Doctoral dissertation), University of Colorado at Boulder, 2021.
[2] N. Shahrubudin, T. Lee, R. Ramlan, An Overview on 3D Printing Technology: Technological, Materials, and Applications, Procedia Manufacturing. 35 (2019) 1286–1296.
[3] A.O. Watanabe, K. Kanno, H. Ito, R.R. Tummala, M. Swaminathan, High-density low-loss millimeter-wave package interconnects with the impact of dielectric-material surface roughness, Applied Physics Letters. 119 (13) (2021) 134103–134111.
[4] S. Juneja, R. Pratap, R. Sharma, Semiconductor technologies for 5G implementation at millimeter wave frequencies – Design challenges and current state of work, Engineering Science and Technology, an International Journal. 24 (1) (2021) 205–217.
[5] G. Gold, Helmreich, K.A physical surface roughness model and its applications, IEEE Trans. Microwave Theory Tech. 65 (2017) 3720–3732.
[6] M.W. Sabri, N.A. Murad, M.K.A. Rahim, Highly directive 3D-printed dual-beam waveguide slotted antennas for millimeter-wave applications, Microwave and Optical Technology Letters. 61 (6) (2019) 1566–1573.
[7] V.T. Le, D.S. Mai, T.K. Doan, H. Paris, Wire and arc additive manufacturing of 308L stainless steel components: Optimization of processing parameters and material properties, Engineering Science and Technology, an International Journal. 24 (4) (2021) 1015–1026.
[8] V. Kyovtorov, I. Georgiev, S. Margenov, D. Stoychev, F. Oliveri, D. Tarchi, Antenna design approach – 3D polymer printing and metallization. experimental test at 14–18GHz, AEU - International Journal of Electronics and Communications. 73 (2017) 119–128.
[9] N.A. Jafar, L.E. Ooi, Z.M. Ripin, K. Ho, A.F. Yahaya, Resistance end correction factor of microperforated panel made using additive manufacturing, Engineering Science and Technology, an International Journal. 24 (6) (2021) 1281–1291.
[10] M.M. Honari, R. Mirzavand, H. Saghlatoon, P. Mousavi, Investigation of the 3D Printing Roughness Effect on the Performance of a Dielectric Rod Antenna, Antennas Wirel. Propag. Lett. 17 (11) (2018) 2075–2079.
[11] J. Romeu, S. Blanch, N. Vidal, J.M. Lopez-Villegas, A. Aguasca, Assessment of 3-D Printing Technologies for Millimeter-Wave Reflectors, IEEE Antennas and Wireless Propagation Letters. 17 (11) (2018) 2061–2064.
[12] B. Zhang, R. Li, L. Wu, H. Sun, Y.X. Guo, A Highly Integrated 3-D Printed Metallic K-Band Passive Front End as the Unit Cell in a Large Array for Satellite Communication, IEEE Antennas and Wireless Propagation Letters. 17 (11) (2018) 2046–2050.
[13] J. Sorocki, I. Piekarz, Low-Cost Microwave Components' Fabrication in Hybrid Technology of Laminates and Additive Manufacturing on an Example of Miniaturized Suspended Directional Coupler, IEEE Access. 8 (2020) 128766–128775.
[14] M.W. Almeshehe, N.A. Murad, M.K.A. Rahim, O. Ayop, F. Zubir, M.Z.A.A. Aziz, M. N. Osman, H.A. Majid, Low loss waveguide-based Butler matrix with iris coupling control method for millimeterwave applications, Waves in Random and Complex Media. (2021) 1–21. online access.
[15] J.G. Hong, M.J. Lancaster, Microstrip Filters for RF/Microwave Applications, (1st ed.)., Wiley-Interscience, 2001.
[16] M.G. Sanchez, Millimeter-Wave (mmWave), *Communications*. Mdpi AG. (2020).
[17] M.W. Sabri, M.K.A. Rahim, F. Zubir, 3D printed horn antenna using direct metal laser melting technique for millimetre wave applications, Indonesian Journal of Electrical Engineering and Informatics (IJEEI). 7 (2) (2019) 323–330.
[18] D.J. Whitehouse, Surfaces and their Measurement (Kogan Page Science Paper Edition), Butterworth-Heinemann, 2004.
[19] R.N. Simons, C.T. Chevalier, E.G. Wintucky, J.C. Freeman, Ka-band waveguide hybrid combiner for MMIC amplifiers with unequal and arbitrary power output ratio, IEEE MTT-S International Microwave Symposium Digest. 2009 (2009) 1–4.
[20] T. Despoisse, N. Deltimple, A. Ghiotto, M. De Matos, J. Forest, P. Busson, An Integrated 65-nm CMOS SOI Ka-Band Asymmetrical Single-Pole Double-Throw Switch Based on Hybrid Couplers, IEEE Microwave and Wireless Components Letters. 30 (12) (2020) 1157–1160.
[21] Z. Zhao, T.A. Denidni, Millimeter-Wave Printed-RGW Hybrid Coupler With Symmetrical Square Feed, IEEE Microwave and Wireless Components Letters. 30 (2) (2020) 156–159.
[22] A. Alaqeel, S. Almorqi, O.M. Haraz, S.A. Alshebeili, A.-R. Sebak, Design of Multilayered K-Band and Ka-Band Slot-Coupled Microstrip 90° Hybrid Couplers Employing Circular Ring Patch Shapes, Wireless Personal Communications. 92 (2) (2017) 653–666.
[23] K. Lomakin, L. Klein, M. Sippel, K. Helmreich, G. Gold, 3D-Printed 3 dB Hybrid Coupler for D-Band Applications, in: 2020 50th European Microwave Conference (EuMC), 2021, pp. 376–379.
[24] W. Liu, Z. Chen, T. Viola, G.H. Huff, 3-D Printed Directional Couplers in Circular Waveguide, IEEE Microwave and Wireless Components Letters. 31 (6) (2021) 561–564.
[25] K. Lomakin, L. Klein, L. Ringel, J. Ringel, M. Sippel, K. Helmreich, G. Gold, 3D Printed E-Band Hybrid Coupler, IEEE Microwave and Wireless Components Letters. 29 (9) (2019) 580–582.
[26] R.V. Haro-Baez, J.A. Ruiz-Cruz, J. Córcoles, J.R. Montejo-Garai, J.M. Rebollar, A New 4 × 4 Rectangular Waveguide Short-Slot Coupler in 3D Printed Technology at Ku-Band, Electronics. 9 (4) (2020) 610.